IEEE Access
Multidisciplinary | Rapid Review | Open Access Journal

Received December 9, 2021, accepted December 18, 2021, date of publication December 21, 2021,
date of current version December 28, 2021.

Digital Object Identifier 10.1109/ACCESS.2021.3137297

Millimeter-Wave Low Side- and Back-Lobe SIW Filtenna Array Fed by Novel Filtering Power Divider Using Hybrid TE_{101}/TE_{301} Mode SIW Cavities

YU-XING YAN[1], WEI YU[1], AND JIAN-XIN CHEN[1,2], (Senior Member, IEEE)
[1]School of Information Science and Technology, Nantong University, Nantong 226019, China
[2]Nantong Research Institute for Advanced Communication Technologies, Chongchuan, Nantong 226019, China

Corresponding author: Jian-Xin Chen (jjxchen@hotmail.com)

This work was supported in part by the National Natural Science Foundation of China under Grant 62001253, in part by the Natural Science Research Project of Jiangsu Provincial Institutions of Higher Education under Grant 20KJA510002, and in part by the Nantong Basic Science Research Program under Grant JC2020080.

ABSTRACT In this article, a novel and simple design approach of millimeter-wave (mm-wave) low side- and back-lobe substrate integrated waveguide (SIW) filtenna array is investigated by using predefined filtering power divider (FPD). The FPD consists of two coupled SIW cavities operating at TE_{101} and TE_{301} modes, respectively. The TE_{301} mode divides the energy from *Cavity* 1 into three parts equally and three outputs are loaded to *Cavity* 2 for power distribution, making the FPD design simplified. Based on this, the predefined power splitting ratio (1:1:1 and 1:3:1) of the FPDs can be obtained easily by controlling the output external quality factor (Q_e). Accordingly, the side and back lobes of the filtenna array are suppressed by using the proposed FPD with predefined power splitting ratio of 1:3:1. To verify the proposed approach, a 3×3 filtenna array prototype centered at 27.2 GHz is designed, fabricated and measured. The measured results show an impedance bandwidth ($|S_{11}| < -10$ dB) of 1.8 %. The filtenna array performs good gain-passband selectivity with an in-band peak gain of 11.1 dBi, and the side lobe is suppressed more than 20 dB while the front-to-back ratio is over 30 dB. Good agreement is achieved between simulated and measured results.

INDEX TERMS Substrate integrated waveguide (SIW), filtering power divider (FPD), slot antenna array, millimeter-wave (mm-wave), side lobe, back lobe.

I. INTRODUCTION

Millimeter-wave (mm-wave) bands have attracted extensive attention in fifth-generation (5G) communications to provide ultra-fast data rate, low latency and significantly improved spectral efficiency [1], [2]. High gain is generally desirable for the mm-wave antenna to increase transmission distance and the antenna array is commonly applied and has been subject of increased amounts of interest [3]–[7]. Meanwhile, filters are usually used to suppress out-of-band noise due to the high stability required in mm-wave communication front end [8]. To improve the performance of mm-wave system, antenna array and filter as two adjacent elements generally are co-designed recently, which is helpful for achieving the target specifications easily.

The associate editor coordinating the review of this manuscript and approving it for publication was Giorgio Montisci.

The fusion design of antenna array and filter can not only reduce the loss but also optimize the overall performance of the mm-wave front end. To date, filtenna array based on microstrip lines [9], [10], metallic waveguides [11], [12], and substrate integrated waveguide (SIW) [13]–[18] have been developed for mm-wave applications. The patch antenna array achieving the filtering response is realized by vertically coupled microstrip resonator and U-slot resonator [9]. But the loss for the open transmission structure such as microstrip resonator is usually serious in mm-wave band. The filtering reflectarray designed by metal waveguide in [11] can effectively achieve high gain, but it is bulky and difficult to integrate with planar circuits. The SIW can be treated as a bridge between the microstrip line and waveguide in terms of loss and volume. In [13] and [14], the feeding networks of filtenna arrays composed of vertically stacked SIW cavities are designed by the traditional synthesis method

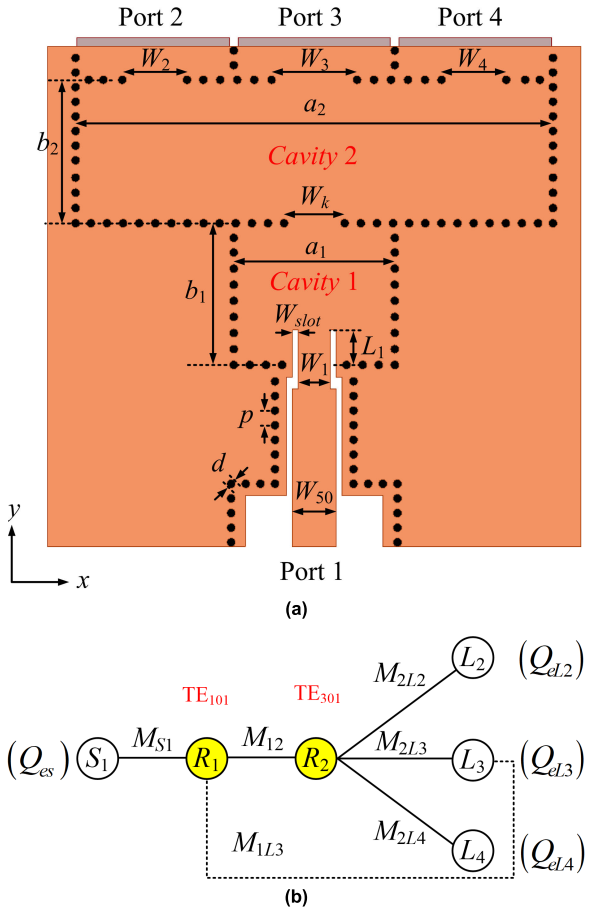

FIGURE 1. The proposed 1-to-3 FPD. (a) Configuration (Design parameters: $d = 0.3$, $p = 0.5$, $a_1 = 5.5$, $b_1 = 4.84$, $a_2 = 16.3$, $b_2 = 4.9$, $W_{50} = 1.48$, $W_1 = 1.08$, $L_1 = 0.51$, $W_2 = W_4 = 2.23$, $W_3 = 2.86$, $W_{slot} = 0.2$ and $W_k = 2.07$. Unit: mm.). (b) Operational topology.

of coupling matrix. However, most of the above mm-wave filtenna arrays are designed with multi-layer structure, which increases the manufacturing cost and complexity. Moreover, the majority of these designs [9]–[18] have high side-lobe levels due to adopting the feeding network with uniform power distribution.

On the other hand, side-lobe level is a key performance characteristics of antenna radiation pattern, which can reduce the waste of radiation energy and suppress electromagnetic interference [19], [20]. A feeding network with unequal power division ratio is one of the important methods to reduce the side lobe of antenna array. The pattern synthesis such as Dolph-Chebyshev distribution [19], Taylor distribution [21] and binomial distribution [22] have been commonly used to reduce the side-lobe level of antenna array. In [23], the feeding network of the X-band filtenna array realizes nonuniform excitation by adjusting the coupling intensity between the last two resonators to achieve low side-lobe level. In mm-wave band, the low side-lobe performance of antenna arrays [24]–[29] is realized by the feeding network with unequal division ratio. However, it is difficult for them to provide filtering response. In [30], a C-band 4-way filtering

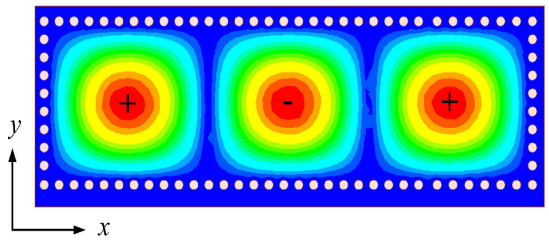

FIGURE 2. Simulated TE_{301} mode E-field distribution of SIW cavity.

power divider (FPD) with predefined division ratio based on half-mode SIW (HMSIW) is presented, where the four outputs are loaded to a single HMSIW resonator. Though the compact size is obtained, its topology is not suitable for applying in mm-wave band because the mm-wave SIW cavity is too small to be loaded by multiple outputs. Accordingly, there is few mm-wave filtenna array with low side lobe are reported so far due to the absence of good FPD with flexible power splitting ratio. In [31], the mm-wave filtenna array achieves low side-lobe level by reducing the distance between the radiating slots, but its design is with low flexibility and only applies to the linear array.

In this paper, a low side- and back-lobe SIW filtenna array with a planar single-layer structure is proposed. The filtenna array is fed by a 1-to-3 SIW FPD with predefined power splitting ratio. In the SIW FPD, both power distribution and filtering response are fulfilled at the same time by using the coupling scheme between TE_{101} mode and TE_{301} mode cavities. Each part of TE_{301} mode answers for one output, and the desired power splitting ratio of the three outputs is determined only by their external quality factor (Q_e) ratio. Accordingly, the predefined power splitting ratio (1:1:1 and 1:3:1) of the FPDs can be obtained easily, and then the FPD with splitting ratio of 1:3:1 is used as the feeding network of slot antenna array. To the best of author knowledge, the feeding network with unequal power splitting ratio is applied for the first time to reduce the side and back lobes of mm-wave filtenna array.

II. DESIGN OF THE MM-WAVE FILTENNA ARRAY

A. DESIGN OF THE FPD USING HYBRID TE_{101}/TE_{301} MODE SIW CAVITIES

Fig. 1(a) shows the geometric configuration of the proposed 1-to-3 FPD, which consists of two coupled SIW resonators (Cavities 1 and 2). Port 1 represents the input while Ports 2, 3 and 4 represent outputs. A 50-Ω grounded coplanar waveguide (GCPW) feeding line is used to excite the TE_{101} modes in Cavity 1. The proposed FPD is designed on a single-layer printed circuit board (PCB), i.e Rogers RT/Duroid 5880 with a relative permittivity of 2.2, a loss tangent of 0.0009 and a thickness of 20 mil. Fig. 1(b) shows the fusion design topology of the proposed FPD. S_1 represents the source (corresponding to Port 1) while L_2, L_3 and L_4 denote the three loads (corresponding to Port 2, Port 3 and Port 4, respectively), where M_{S1}, M_{12}, M_{2L2}, M_{2L3} and M_{2L4} indicated by solid line are the main-coupling items, while M_{1L3} expressed by

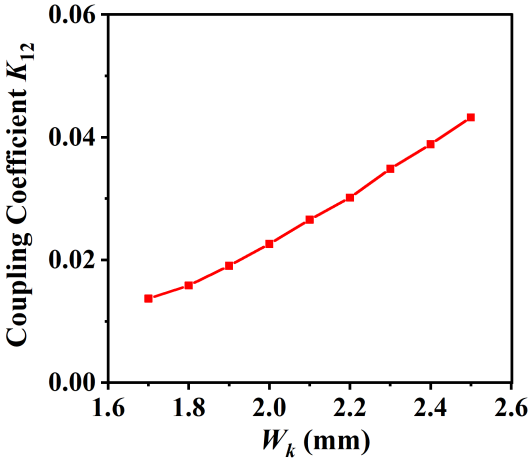

FIGURE 3. Coupling coefficient K_{12} versus the width W_k of coupling window.

dash line is the cross-coupling item. It can be seen from Fig. 1(a) that R_1 is closer to L_3 as compared with L_2 and L_4. Therefore, there is a cross coupling between R_1 and L_3. The coupling matrix M can be expressed as follows:

$$M = \begin{bmatrix} & S & 1 & 2 & L_2 & L_3 & L_4 \\ S & 0 & M_{S1} & 0 & 0 & 0 & 0 \\ 1 & M_{S1} & 0 & M_{12} & 0 & M_{1L3} & 0 \\ 2 & 0 & M_{12} & 0 & M_{2L2} & M_{2L3} & M_{2L4} \\ L_2 & 0 & 0 & M_{2L2} & 0 & 0 & 0 \\ L_3 & 0 & M_{1L3} & M_{2L3} & 0 & 0 & 0 \\ L_4 & 0 & 0 & M_{2L4} & 0 & 0 & 0 \end{bmatrix} \tag{1}$$

The employed SIW Cavities 1 and 2 are designed to resonate at TE_{101} and TE_{301} modes, respectively. Cavity 1 is coupled with Cavity 2 through the coupling window, and the energy from Cavity 1 is equally divided into three parts by the TE_{301} mode in Cavity 2. All three outputs are located at the position of the strongest electric field of TE_{301} mode. Accordingly, both power distribution and filtering response are fulfilled at the same time by using the coupling scheme between TE_{101} mode and TE_{301} mode cavities. The E-field distribution of the operating TE_{301} mode of Cavity 2 is given in Fig. 2. The plus (+) and minus (-) signs indicate the orientation of the E-field. It can be seen that the phase in the middle of TE_{301} mode is opposite to the two sides.

The resonant frequency of TE_{m0q}-mode can be easily determined by (2) [32]

$$f_{TE_{m0q}} = \frac{c}{2\sqrt{\mu_r \varepsilon_r}} \sqrt{\left(\frac{m}{a}\right)^2 + \left(\frac{q}{b}\right)^2} \tag{2}$$

where c is the velocity of light in vacuum, μ_r and ε_r are the relative permeability and relative permittivity of the dielectric substrate, m and q are the mode indices along the respective x-axis and y-axis directions. a and b denote the length and width of the SIW cavity, respectively.

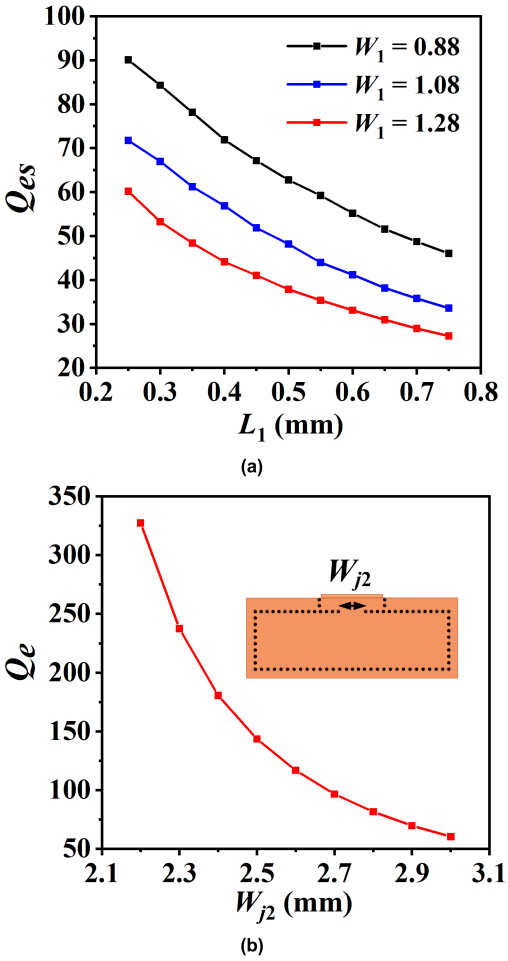

FIGURE 4. The extracted Q_e. (a) Q_e versus L_1 with different W_1. (b) Q_e versus W_{j2} for the loads.

Assuming that the multiport network in Fig. 1(b) is lossless, and P_1 and P_i ($i = 2, 3$ or 4) represent the input power of *Cavity* 1 and the dissipated power of each output of *Cavity* 2, we can obtain the $P_1 = P_2 + P_3 + P_4$. The power splitting ratio and the dissipated power of each output are defined as

$$P_2 : P_3 : P_4 = \alpha_2 : \alpha_3 : \alpha_4 \tag{3}$$

$$P_i = \frac{\alpha_i}{\sum_{i=2}^{4} \alpha_i} P_1 \tag{4}$$

According to the definition of the Q_e, the input Q_{es} and the Q_{eLi} of each output can be expressed as

$$Q_{es} = \omega_0 \frac{W_a}{P_1} \tag{5}$$

$$Q_{eLi} = \omega_0 \frac{W_a}{P_i} \tag{6}$$

where W_a and ω_0 represent the average energy storage and the resonant frequency of the employed resonator, respectively.

Accordingly, we can obtain each output Q_{eLi}

$$Q_{eLi} = \frac{\sum_{i=2}^{4} \alpha_i}{\alpha_i} Q_{es} \tag{7}$$

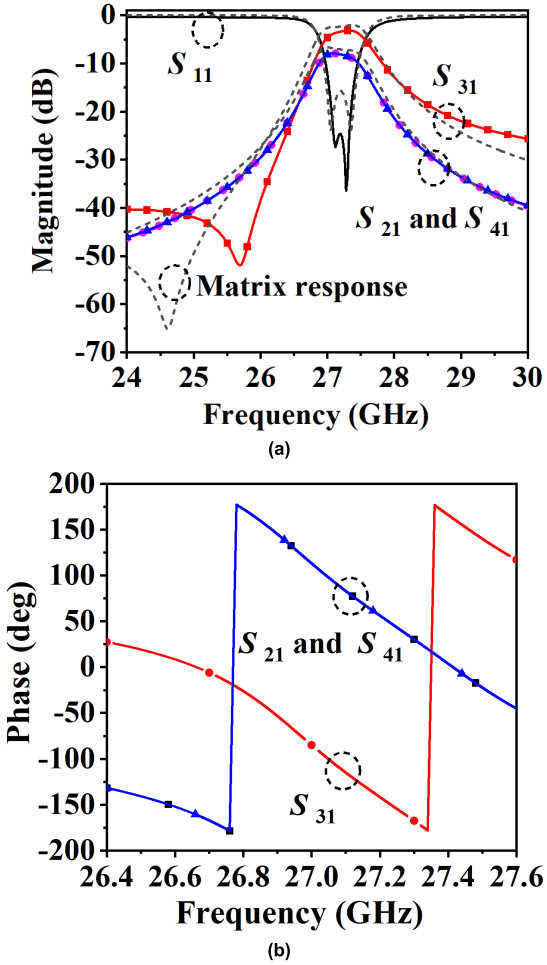

FIGURE 5. Simulated results of the proposed FPD with predefined power splitting ratio of 1:1:1. (a) Magnitude (Simulated and matrix response). (b) Phase-frequency response.

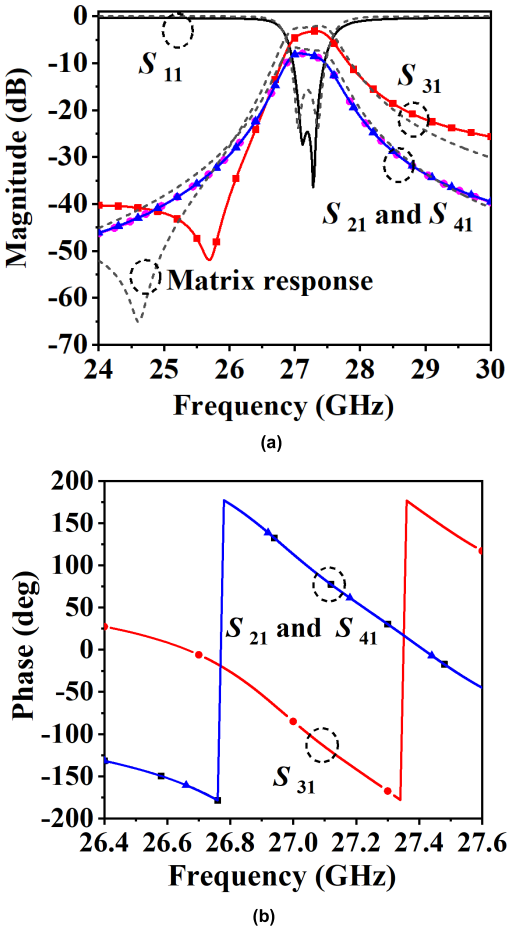

FIGURE 6. Simulated results of the proposed FPD with predefined power splitting ratio of 1:3:1. (a) Magnitude (Simulated and matrix response). (b) Phase-frequency response.

It is can be found the Q_e ratio obtained in this way is consistent with the relationship between the Q_e and power splitting ratio in [33]. For example, when the in-band splitting ratio is set as α_2: α_3: $\alpha_4 = 1{:}1{:}1$, the three output Q_e is equal and can be calculated as $Q_{eL2} = Q_{eL3} = Q_{eL4} = 3Q_{es}$.

Based on the above discussion, the design process of the proposed second-order FPD can be divided into two steps, which can be synthesized independently. In the first step, according to the specification of filtering, the desired input Q_{es} and coupling coefficient K_{12} can be determined by the lumped parameters of a lowpass prototype.

$$Q_{es} = \frac{g_0 g_1}{FBW} \tag{8}$$

$$K_{12} = \frac{FBW}{\sqrt{g_1 g_2}} \tag{9}$$

The second step is to split in-band power by controlling each output Q_e by using (7). To demonstrate the above derived theory, two design examples with predefined splitting ratios are designed.

The first example is an mm-wave 1-to-3 FPD with splitting ratio 1:1:1, and the passband response is with center frequency $f_0 = 27.2$ GHz and 0.1-dB-ripple fractional bandwidth (FBW) of about 1.65% in this design. ($g_0 = 1$, $g_1 = 0.8431$, and $g_2 = 0.6220$). Thus, the desired input $Q_{es} = 51.1$ and $K_{12} = 0.023$, meanwhile, the output $Q_{eLi} = 3Q_{es} = 153.3$.

Fig. 3 shows the design curve of K_{12} of the proposed FPD, which can be used to determine the window length W_k. The main-coupling parameters M_{12} and M_{S1} can be obtained by

$$M_{12} = \frac{K_{12}}{FBW} \tag{10}$$

$$M_{S1} = \frac{1}{FBW \cdot Q_{es}} \tag{11}$$

According to (7), in order to achieve the splitting ratio of 1:1:1, there must be

$$M_{2Li} = \frac{1}{\sqrt{FBW \cdot Q_{eLi}}} (i = 2, 3, 4) \tag{12}$$

The coupling matrix M_1 of the proposed 1:1:1 FPD is synthesized as shown in (13), as shown at the bottom of the next page.

Fig. 4(a) shows the curve of input Q_{es} against L_1 and W_1 when other parameters are fixed. It is found that when the Q_{es} decreases as L_1 or W_1 is increased. In other words, the Q_{es} is

reduced when the coupling strength between the *Cavity* 1 and the feeding line increases. For the three outputs, it can be seen from Fig. 2 that the energies of the three parts of TE_{301} mode are equal so that only one output Q_e needs to be extracted in this design, as shown in Fig. 4(b), where the output is located at the center of the SIW *Cavity* 2. The value of Q_e decreases as W_{j2} increases. The Q_e values of the other outputs (Ports 2 and 4) are referred to Fig. 4(b). As a result, the three output coupling windows (W_2, W_3 and W_4) are equal in this case. Accordingly, the final dimensions of the proposed FPD can be determined after fine tuning.

Fig. 5 shows the simulated results of the FPD, verifying the simple design procedure is effective. It can be seen the matrix response and simulated result match each other in the passband. Owing to cross coupling, a transmission zero is generated on the side of the lower stopband of S_{31}.

For further demonstration, a FPD with unequal splitting ratio of 1:3:1 is designed, which will be used as a feeding network of filtenna array for achieving low side lobe. This FPD has the same filtering specifications as the first example above. Thus, the desired input $Q_{es} = 51.1$ and $K_{12} = 0.023$, meanwhile, the output $Q_{eL2} = Q_{eL4} = 255.5$, and $Q_{eL3} = 85.2$. The coupling matrix M_2 to achieve the division ratio of 1:3:1 can be synthesized in (14), as shown at the bottom of the page, where M_{S1} in the coupling matrix M_2 is consistent with that in (10), the other main-coupling parameters can be expressed as

$$M_{2Li} = \frac{1}{\sqrt{FBW \cdot 5Q_{es}}} (i = 2, 4) \tag{15}$$

$$M_{2L3} = \frac{1}{\sqrt{FBW \cdot \frac{5}{3}Q_{es}}} \tag{16}$$

The simulated results of the FPD with splitting ratio of 1:3:1 are shown in Fig. 6. According to the unequal power splitting ratio of 1:3:1, the ideal S_{21}, S_{31}, and S_{41} are −6.99 dB, −2.22 dB and −6.99 dB, respectively. As can be seen from Fig. 6(a), the simulated results show that the FPD centered at f_0 owns a 3-dB *FBW* of 2.24%. The simulated

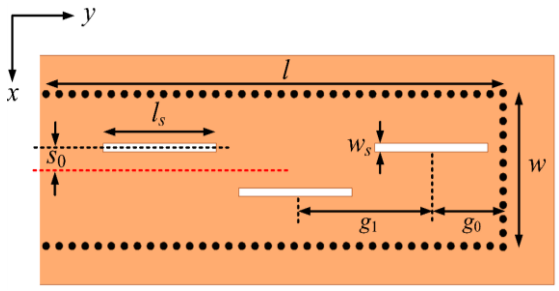

FIGURE 7. Configuration of the 1 × 3 slot subarray. (Design parameters: $l = 18.0$, $w = 5.43$, $w_s = 0.3$, $s_0 = 0.25$, $l_s = 4.33$, $g_1 = 5.2$ and $g_0 = 2.75$. Unit: mm.)

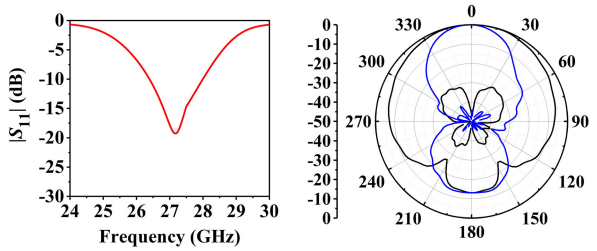

FIGURE 8. Simulated results of the 1 × 3 SIW slot subarray. (a) $|S_{11}|$. (b) Radiation patterns (*E*-plane: black curves, *H*-plane: blue curves).

reflection coefficient ($|S_{11}|$) is better than 20 dB within the passband, and the simulated insertion loss for the three paths is about 1.2 dB (not including 1:3:1 power division loss). And a transmission zero is generated at 24.6 GHz in the lower stopband of S_{31} due to the cross coupling (M_{1L3}). Fig. 5(b) and Fig. 6(b) show the phase-frequency responses of the outputs. As expected, Port 2 and Port 4 are in-phase and Port 3 is out-of-phase. This method of using Q_e to control power distribution is independent of the output phase of the FPD.

B. DESIGN OF THE SIW SLOT ANTENNA ARRAY

Fig. 7 illustrates the 1 × 3 SIW slot subarray that is fed with a waveguide port. The structure of SIW slot array in longitudinal direction is similar to that of the conventional

$$M_1 = \begin{bmatrix} & S & 1 & 2 & L_2 & L_3 & L_4 \\ S & 0 & 1.0890 & 0 & 0 & 0 & 0 \\ 1 & 1.0890 & 0 & 1.3810 & 0 & -0.0900 & 0 \\ 2 & 0 & 1.3810 & 0 & 0.6287 & 0.6287 & 0.6287 \\ L_2 & 0 & 0 & 0.6287 & 0 & 0 & 0 \\ L_3 & 0 & -0.0900 & 0.6287 & 0 & 0 & 0 \\ L_4 & 0 & 0 & 0.6287 & 0 & 0 & 0 \end{bmatrix} \tag{13}$$

$$M_2 = \begin{bmatrix} & S & 1 & 2 & L_2 & L_3 & L_4 \\ S & 0 & 1.0890 & 0 & 0 & 0 & 0 \\ 1 & 1.0890 & 0 & 1.3810 & 0 & -0.0900 & 0 \\ 2 & 0 & 1.3810 & 0 & 0.4870 & 0.8435 & 0.4870 \\ L_2 & 0 & 0 & 0.4870 & 0 & 0 & 0 \\ L_3 & 0 & -0.0900 & 0.8435 & 0 & 0 & 0 \\ L_4 & 0 & 0 & 0.4870 & 0 & 0 & 0 \end{bmatrix} \tag{14}$$

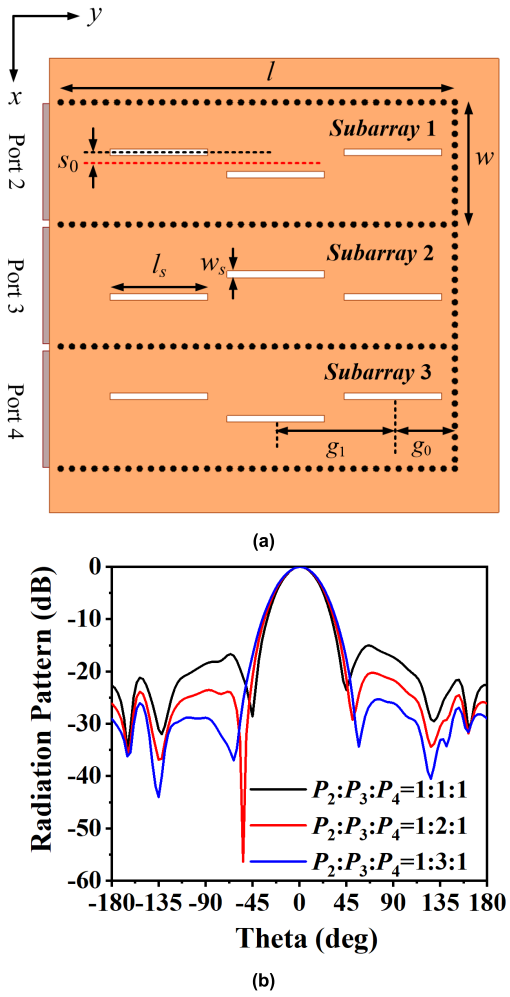

FIGURE 9. The proposed 3 × 3 SIW slot array. (a) Configuration. (b) Simulated radiation patterns of the 3 × 3 antenna array in *E*-plane with different incident power ratio at f_0.

waveguide slot array [34]. In SIW slot array structures, the calculation of parameters is slightly different from that of rectangular waveguide due to the built-in medium [35]. The initial antenna width w is about $0.5\lambda_0$(λ_0 is free space wavelength at f_0). In this design, three longitudinal slots are intermittently placed at the two sides of the center line. In order to obtain the low side lobes of both *E*- and *H*-planes in the final filtenna array, the adjacent slots along the *y*-axis are spaced at about half of guided wavelength ($\lambda_g/2$) for achieving zero side lobe of *H*-plane [28], as shown in Fig. 8, at the expense of slight gain reduction. The distance between the last slot along the *y*-axis is $\lambda_g/4$ from the right short plane for matching. As can be seen from Fig. 8 (a), the simulated *FBW* ($|S_{11}| < -10$ dB) of the 1 × 3 subarray at $f_0 = 27.2$ GHz is 5.9 % (26.39 - 27.99 GHz). The simulated radiation patterns are presented in Fig. 8(b).

On this basis, the 1 × 3 subarray in Fig. 8 is used to construct a 3 × 3 slot antenna array, which is realized by placing 3 subarrays along the *x*-axis for constructing an array in *E*-plane. The specific configuration of 3 × 3 antenna

TABLE 1. Side- and back-lobe comparison of 3 × 3 antenna array with different power ratio.

Incident Power Ratio	f_0 (GHz)	Side-lobe Suppression (dB)	FTBR (dB)	In-band Peak Gain (dBi)
1:1:1	27.2	15.01	22.63	13.92
1:2:1		20.23	26.13	13.87
1:3:1		29.03	29.03	13.73

FTBR: Front-to-back ratio.

array is shown in Fig. 8 (a), where inputs are Port 2, 3 and 4 correspond to the outputs of FPD in Fig. 1. To radiate in-phase, the slots of the *Subarray* 2 should be positioned alternately opposite to slots in *Subarrays* 1 and 3 (with respect to the central red line) because the phase difference between Port 3 and Port 2/Port 4 is 180°, as can be seen from Fig. 6(b). The excitation powers of the three inputs of the 3 × 3 antenna array are P_2, P_3 and P_4 respectively. The simulated radiation patterns of the antenna array in *E*-plane with different power ratios at f_0 are given in Fig. 9 (b) (here the proposed FPD is not included). It confirms the side-lobe level suppression when high energy is placed on the middle subarray. In addition, it can be seen that the utilization of unequal power distribution results in a low back-lobe antenna array. This is because the middle subarray (*Subarray* 2) shown in Fig. 9 acquiring the highest power owns the largest reflecting ground plane. It can be seen from Fig. 10 that the E-field in the middle subarray of slot antenna array is strongest due to the power division ratio of FPD is set as 1:3:1. Table 1 shows the influence of power splitting ratio on side and back lobes of antenna array in *E*-plane. Both side- and back-lobes are suppressed more than 25 dB when the power division ratio is set as 1:3:1. Fig. 10 shows the photograph of the implemented 3 × 3 filtenna array prototype. The occupied area of the filtenna array is 28.9 mm × 17.5 mm (2.62 λ_0× 1.59 λ_0). The 1-to-3 SIW FPD provides three paths to directly excite the proposed 3 × 3 antenna array, showing simple design procedure.

III. RESULTS AND DISCUSSION

The radiation performance is measured using the mm-wave antenna measurement system in a chamber as shown in Fig. 12. The input signal is generated by an Agilent signal generator E8257D and is fed to a standard horn antenna (26.5-40 GHz). The employed spectrum analyzer is Agilent E4447A.

Fig. 13 exhibits the simulated and measured $|S_{11}|$ and gain of the proposed 3 × 3 filtenna array. It can be found that the measured FBW ($|S_{11}| < -10$ dB) is 1.8 % (26.87 - 27.35 GHz). The measured peak gain is 11.1 dBi, and the in-band gain curve is flat. As can be seen, the out-of-band rejection of the gain is good in this design. The suppression is more than 13.5 dB at stopband frequency above 28 GHz while it reaches 26 dB at the stopband

TABLE 2. Comparison of the proposed filtenna array with other previous designs.

Ref.	f_0 (GHz)	Array Scale	Technology	FBW (%)	Return Loss (dB)	Peak Gain (dBi)	Side-lobe Suppression (dB)	FTBR (dB)	ξ (dB/GHz)	Filtering Response	Power Division Ratio	Size ($\lambda_0 \times \lambda_0$)
[12]	34.0	2 × 2	Waveguide	2.9	>15	12.5	8.1	16.5	7.5	Yes	Equal	1.46 × 1.46
[13]	37.0	2 × 2	SIW	1.6	>15	10.8	12.0	16.0	48.6	Yes	Equal	2.34 × 2.34
[14]	29.3	1 × 4	SIW	1.2	>11	8.1	N.A.	N.A.	15.0	Yes	Equal	2.08 × 1.67
[15]	28.0	1 × 4	SIW	5.0	>10	11.1	15.5	20.0	3.0	Yes	Equal	3.08 × 2.52
[24]	28.3	1 × 8	SIW	8.1	>15	14.0	20.0	>25.0	N.A.	No	Unequal	6.54 × 5.93
[29]	77	3 × 8	SIW	7.0	>10	16.0	24.0	N.A.	N.A.	No	Unequal	7.71 × 1.36
This work	27.2	3 × 3	SIW	1.8	>15	11.1	20.0	>30	17.0	Yes	Unequal	2.62 × 1.59

Gain roll-off ξ is defined as:

$$\xi = \frac{G_{3dB} - G_{20dB}}{|f_{3dB} - f_{20dB}|} \text{ (dB/GHz)}$$

where $G_{3dB} = G_{max}$ -3 dB and $G_{20dB} = G_{max}$ -20 dB (G_{max} is the peak gain in the passband), while f_{3dB} and f_{20dB} represent the 3dB and 20dB cutoff frequency of the gain passband, respectively.

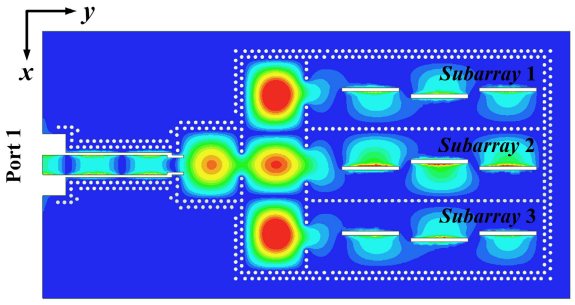

FIGURE 10. Simulated E-field distribution of the proposed SIW filtenna array at f_0.

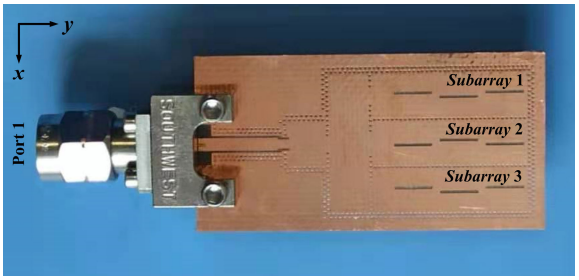

FIGURE 11. Photograph of the proposed SIW filtenna array.

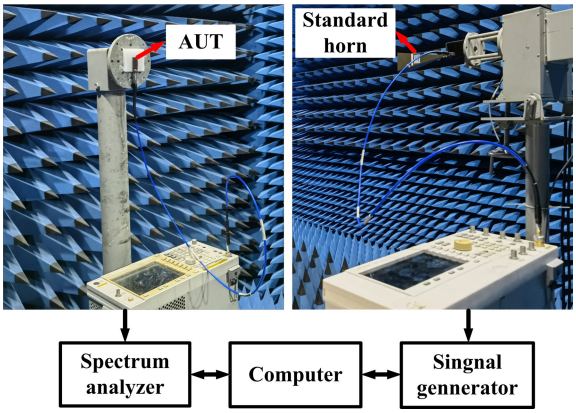

FIGURE 12. The measurement setup for the proposed antenna array.

below 26 GHz. Fig. 14 shows the simulated and measured radiation patterns of the proposed 3 × 3 filtenna array at f_0. The cross-polarization (x-pol) levels are lower than −20 dB in both E-plane and H-plane. All side-lobe levels of the measured realized radiation patterns are less than −20 dB. The measured front-to-back-ratio (FTBR) is more than 30 dB, indicating that unequal power division feeding technique is a feasible approach to reduce both side- and back-lobe levels simultaneously. It is well known that the mm-wave antenna is very sensitive to the fabrication and implementation errors and the testing environment such as turntable and cable will also affect the radiation patterns. As shown in Fig. 14, the average error between the measured and simulated radiation patterns is only 0.5 dB within the 3 dB beamwidths of E- and H-planes, showing good consistency. Meanwhile, the average error becomes large (the maximum difference is 5.8 dB) at beam pointing angles of 30° to 90° and 270° to 330°. This is because the signal received by the spectrum analyzer in Fig. 12 is very small due to the short wavelength of millimeter waves at these angles, and then the spectrum analyzer records the received RF power, whose fluctuation is large but the

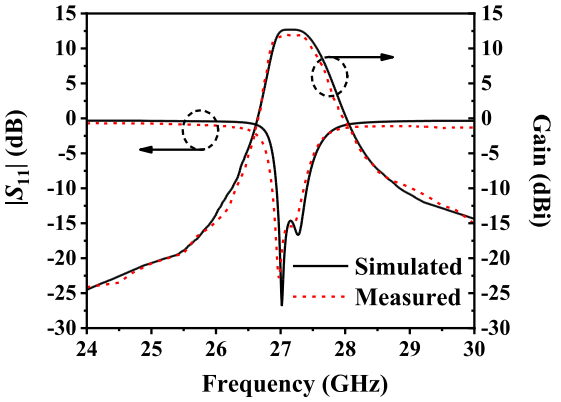

FIGURE 13. Comparison of the measured and simulated gain curves and $|S_{11}|$ responses of the proposed filtenna array.

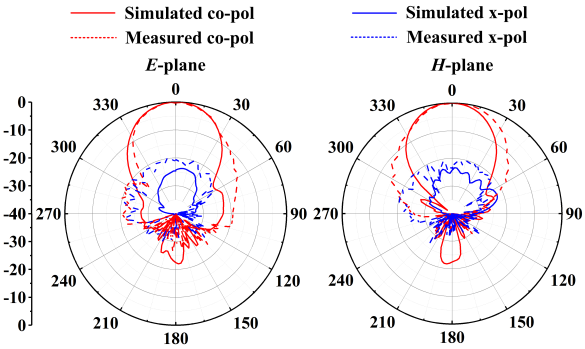

FIGURE 14. Simulated and measured filtenna array radiation patterns at f_0.

power difference is small. As a whole, the measured radiation patterns of the proposed antenna array agree well with the simulated ones, which verify the proposed design concept effectively.

The comparisons of the proposed filtenna array with previously reported counterparts are summarized and listed in Table 2. Benefiting from the adoption of the unequal power division ratio, the filtenna array has the lowest side and back lobes as compared with the reported filtenna arrays using equal power dividers [12]–[15]. In [12], the filtenna array has higher gain, but the low-loss waveguide structure is used, which is bulky and not suitable to integrate with planar circuits. In [13], it is reasonable that the gain roll-off (ξ) of the filtenna array is high due to the four resonators are applied in achieving bandpass response. It can also be seen from [24] and [29] that the feeding network with unequal power ratio are effective in reducing the sidelobe of antenna array, but neither of these two designs can provide filtering response.

IV. CONCLUSION

In this article, a single-layer low side- and back-lobe mm-wave SIW filtenna array fed by FPD with predefined power splitting ratio has been presented, and the design procedure and parametric studies have been given in detail. The SIW filtenna array is realized in a simple and straightforward way by directly connecting the FPD to the antenna array, achieving low side and back lobes. The proposed 3 × 3 filtenna array has several advantages such as simple structure, easy fabrication, and high performance. Therefore, it would be an attractive candidate for the applications in mm-wave wireless communication systems.

REFERENCES

[1] W. Hong, Z. H. Jiang, C. Yu, D. Hou, H. Wang, C. Guo, Y. Hu, L. Kuai, Y. Yu, Z. Jiang, Z. Chen, J. Chen, Z. Yu, J. Zhai, N. Zhang, L. Tian, F. Wu, G. Yang, Z.-C. Hao, and J. Y. Zhou, "The role of millimeter-wave technologies in 5G/6G wireless communications," *IEEE J. Microw.*, vol. 1, no. 1, pp. 101–122, Jan. 2021.

[2] A. N. Uwaechia and N. M. Mahyuddin, "A comprehensive survey on millimeter wave communications for fifth-generation wireless networks: Feasibility and challenges," *IEEE Access*, vol. 8, pp. 62367–62414, 2020.

[3] J. Zhu, C.-H. Chu, L. Deng, C. Zhang, Y. Yang, and S. Li, "mm-Wave high gain cavity-backed aperture-coupled patch antenna array," *IEEE Access*, vol. 6, pp. 44050–44058, 2018.

[4] N. Ashraf, A.-R. Sebak, and A. A. Kishk, "PMC packaged single-substrate 4 × 4 Butler matrix and double-ridge gap waveguide horn antenna array for multibeam applications," *IEEE Trans. Microw. Theory Techn.*, vol. 69, no. 1, pp. 248–261, Jan. 2021.

[5] J. Xiao, Z. Qi, X. Li, and H. Zhu, "Broadband and high-gain SIW-fed slot array for millimeter-wave applications," *IEEE Trans. Antennas Propag.*, vol. 67, no. 5, pp. 3484–3489, May 2019.

[6] J. Zhu, S. Li, S. Liao, and B.-L. Bu, "High-gain series-fed planar aperture antenna array," *IEEE Antennas Wireless Propag. Lett.*, vol. 16, pp. 2750–2754, 2017.

[7] S. M. Sifat, M. M. M. Ali, S. I. Shams, and A.-R. Sebak, "High gain bow-tie slot antenna array loaded with grooves based on printed ridge gap waveguide technology," *IEEE Access*, vol. 7, pp. 36177–36185, 2019.

[8] H. Zhu, X. Zhu, Y. Yang, and Q. Xue, "Design of wideband third-order bandpass filters using broadside-coupled resonators in 0.13-μm (bi)-CMOS technology," *IEEE Trans. Microw. Theory Techn.*, vol. 66, no. 12, pp. 5593–5604, Dec. 2018.

[9] C.-X. Mao, S. Gao, and Y. Wang, "Broadband high-gain beam-scanning antenna array for millimeter-wave applications," *IEEE Trans. Antennas Propag.*, vol. 65, no. 9, pp. 4864–4868, Sep. 2017.

[10] X. Xu, M. Zhang, J. Hirokawa, and M. Ando, "E-band plate-laminated waveguide filters and their integration into a corporate-feed slot array antenna with diffusion bonding technology," *IEEE Trans. Microw. Theory Techn.*, vol. 64, no. 11, pp. 3592–3603, Nov. 2016.

[11] G. Wu, Y. S. Zeng, K. F. Chan, B. J. Chen, S. W. Qu, and C. H. Chan, "High-gain filtering reflectarray antenna for millimeter-wave applications," *IEEE Trans. Antennas Propag.*, vol. 68, no. 2, pp. 805–812, Feb. 2020.

[12] X. He, Y. Zhang, M. Du, and J. Xu, "Lightweight and compact high-gain filtering aperture antenna fabricated by three-dimensional printing technology," *IEEE Antennas Wireless Propag. Lett.*, vol. 17, no. 7, pp. 1141–1144, Jul. 2018.

[13] H. Chu and Y.-X. Guo, "A filtering dual-polarized antenna subarray targeting for base stations in millimeter-wave 5G wireless communications," *IEEE Trans. Compon., Packag., Manuf. Technol.*, vol. 7, no. 6, pp. 964–973, Jun. 2017.

[14] H. Chu, J.-X. Chen, S. Luo, and Y.-X. Guo, "A millimeter-wave filtering monopulse antenna array based on substrate integrated waveguide technology," *IEEE Trans. Antennas Propag.*, vol. 64, no. 1, pp. 316–321, Jan. 2016.

[15] H. Jin, G. Q. Luo, W. Wang, W. Che, and K.-S. Chin, "Integration design of millimeter-wave filtering patch antenna array with SIW four-way anti-phase filtering power divider," *IEEE Access*, vol. 7, pp. 49804–49812, 2019.

[16] H.-T. Hu and C. H. Chan, "Substrate-integrated-waveguide-fed wideband filtering antenna for millimeter-wave applications," *IEEE Trans. Antennas Propag.*, vol. 69, no. 12, pp. 8125–8135, Dec. 2021, doi: 10.1109/TAP.2021.3083777.

[17] J. Zhang, S. Zhang, and G. F. Pedersen, "Dual-band structure reused antenna based on quasi-elliptic bandpass frequency selective surface for 5G application," *IEEE Trans. Antennas Propag.*, vol. 68, no. 11, pp. 7612–7617, Nov. 2020.

[18] R. Lu, C. Yu, F. Wu, Z. Yu, L. Zhu, J. Zhou, P. Yan, and W. Hong, "SIW cavity-fed filtennas for 5G millimeter-wave applications," *IEEE Trans. Antennas Propag.*, vol. 69, no. 9, pp. 5269–5277, Sep. 2021.
[19] K. Xing, B. Liu, Z. Guo, X. Wei, R. Zhao, and Y. Ma, "Backlobe and sidelobe suppression of a *Q*-band patch antenna array by using substrate integrated coaxial line feeding technique," *IEEE Antennas Wireless Propag. Lett.*, vol. 16, pp. 3043–3046, 2017.
[20] W. Lin and R. W. Ziolkowski, "Compact, highly efficient Huygens antenna array with low sidelobe and backlobe levels," *IEEE Trans. Antennas Propag.*, vol. 69, no. 10, pp. 6401–6409, Oct. 2021.
[21] X. Jiang, F. Jia, Y. Cao, P. Huang, J. Yu, X. Wang, and Y. Shi, "Ka-band 8 × 8 low-sidelobe slot antenna array using a 1-to-64 high-efficiency network designed by new printed RGW technology," *IEEE Antennas Wireless Propag. Lett.*, vol. 18, no. 6, pp. 1248–1252, Jun. 2019.
[22] R. Chopra and G. Kumar, "Series-fed binomial microstrip arrays for extremely low sidelobe level," *IEEE Trans. Antennas Propag.*, vol. 67, no. 6, pp. 4275–4279, Jun. 2019.
[23] F.-C. Chen, J.-F. Chen, Q.-X. Chu, and M. J. Lancaster, "X-band waveguide filtering antenna array with nonuniform feed structure," *IEEE Trans. Microw. Theory Techn.*, vol. 65, no. 12, pp. 4843–4850, Dec. 2017.
[24] S.-J. Park, D.-H. Shin, and S.-O. Park, "Low side-lobe substrate-integrated-waveguide antenna array using broadband unequal feeding network for millimeter-wave handset device," *IEEE Trans. Antennas Propag.*, vol. 64, no. 3, pp. 923–932, Mar. 2016.
[25] A. Dewantari, J. Kim, I. Scherbatko, and M.-H. Ka, "A sidelobe level reduction method for mm-wave substrate integrated waveguide slot array antenna," *IEEE Antennas Wireless Propag. Lett.*, vol. 18, no. 8, pp. 1557–1561, Aug. 2019.
[26] J. Liu, F. Yang, K. Fan, and C. Jin, "Unequal power divider based on inverted microstrip gap waveguide and its application for low sidelobe slot array antenna at 39 GHz," *IEEE Trans. Antennas Propag.*, vol. 69, no. 12, pp. 8415–8425, Dec. 2021, doi: 10.1109/TAP.2021.3096981.
[27] Y. He, K. Ma, N. Yan, Y. Wang, and H. Zhang, "A cavity-backed endfire dipole antenna array using substrate-integrated suspended line technology for 24 GHz band applications," *IEEE Trans. Antennas Propag.*, vol. 66, no. 9, pp. 4678–4686, Sep. 2018.
[28] D. Wang, Y. J. Cheng, S. C. Jin, S. H. Zhang, S. S. Yao, L. Wang, and Y. Fan, "W-band low-SLL size-reduction microwaveguide array antenna using TE_{120}-mode-cavity dual-layer power divider," *IEEE Antennas Wireless Propag. Lett.*, vol. 20, no. 11, pp. 2146–2150, Nov. 2021, doi: 10.1109/LAWP.2021.3106657.
[29] T. Djerafi, A. Patrovsky, K. Wu, and S. O. Tatu, "Recombinant waveguide power divider," *IEEE Trans. Microw. Theory Techn.*, vol. 61, no. 11, pp. 3884–3891, Nov. 2013.
[30] Y. Yan, W. Yu, W. Qin, M. Du, and J. Chen, "Compact HMSIW four-way filtering power divider with pre-defined division ratio," *Int. J. RF Microw. Comput.-Aided Eng.*, vol. 31, no. 10, pp. 1–7, Oct. 2021.
[31] X. Liu, H. Wang, S. Quan, X. Jiang, W. Xu, and D. Xu, "Design of a *W* band filter antenna array with low sidelobe level using gap waveguide," in *Proc. 11th Int. Symp. Antennas, Propag. EM Theory (ISAPE)*, Guilin, China, Oct. 2016, pp. 132–134.
[32] D. M. Pozar, *Microwave Engineering*, 3rd ed. New York, NY, USA: Wiley, 2005, ch. 6, sec. 3, pp. 278–279.
[33] W. Yu, W. Qin, and J.-X. Chen, "Theory and experiment of multiport filtering power divider with arbitrary division ratio based on dielectric resonator," *IEEE Trans. Ind. Electron.*, vol. 66, no. 1, pp. 407–415, Jan. 2019.
[34] S. H. Zhong, *Antenna Theory and Technique*, 2rd ed. Beijing, China: Publishing House of Electronics Industry, 2015, ch. 6, sec. 1, pp. 245–246.
[35] A. A. Diman, F. Karami, P. Rezaei, A. Amn-e-Elahi, Z. Mousavirazi, T. A. Denidni, and A. A. Kishk, "Efficient SIW-feed network suppressing mutual coupling of slot antenna array," *IEEE Trans. Antennas Propag.*, vol. 69, no. 9, pp. 6058–6063, Sep. 2021.

YU-XING YAN was born in Tongchuan, Shaanxi, China, in 1999. She received the B.E. degree from Nantong University, Nantong, China, in 2021, where she is currently pursuing the M.S. degree in electromagnetic field and microwave technology. Her current research interest includes microwave antenna.

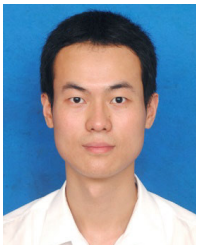

WEI YU was born in Nantong, Jiangsu, China, in 1986. He received the B.S. and M.S. degrees from Nanjing Forestry University, Nanjing, China, in 2009 and 2012, respectively. He is currently pursuing the Ph.D. degree in information and communication engineering with Nantong University, Nantong.

Since 2012, he has been with the Engineering Training Center, Nantong University, where he is also a Lecturer. His research interests include microwave active/passive circuits and antennas.

JIAN-XIN CHEN (Senior Member, IEEE) was born in Nantong, Jiangsu, China, in 1979. He received the B.S. degree from the Huaiyin Teachers College, Huaiyin, Jiangsu, in 2001, the M.S. degree from the University of Electronic Science and Technology of China (UESTC), Chengdu, China, in 2004, and the Ph.D. degree from the City University of Hong Kong, Hong Kong, in 2008.

Since 2009, he has been with Nantong University, where he is currently a Professor. He has authored or coauthored more than 80 internationally referred journal articles and conference papers. He holds three Chinese patents and two U.S. patents. His research interests include microwave active/passive circuits and antennas, and LTCC-based millimeter-wave circuits and antennas. He was a recipient of the Best Paper Award presented at the Chinese National Microwave and Millimeter-Wave Symposium, Ningbo, China, in 2007. He was a Supervisor of 2014 iWEM Student Innovation Competition Winner in Sapporo, Japan.